Ceramics International 46 (2020) 4410–4415

Contents lists available at ScienceDirect

Ceramics International

journal homepage: www.elsevier.com/locate/ceramint

Cd-substituted Mg composites with dual-equivalent permeability and permittivity for high-frequency miniaturization antennas

Gongwen Gan[a], Dainan Zhang[a,*], Jie Li[a], Gang Wang[a], Xin Huang[a], Yan Yang[a], Yiheng Rao[a], Fang Xu[a], Xueying Wang[a], Huaiwu Zhang[a], Ray T. Chen[b,**]

[a] State Key Laboratory of Electronic Thin Films and Integrated Devices, University of Electronic Science and Technology of China, Chengdu, 610054, China
[b] Microelectronic Research Center, Department of Electrical and Computer Engineering, University of Texas at Austin, Austin, TX, 78758, USA

ARTICLE INFO

Keywords:
$Mg_{1-x}Cd_xCo_{0.05}Fe_{1.95}O_4$ composites
Enhanced magnetic properties
Dual-equivalent μ' and ε'
High miniaturization factors
Low loss factors

ABSTRACT

Spinel Mg ferrites $Mg_{1-x}Cd_xCo_{0.05}Fe_{1.95}O_4$ (x = 0.0, 0.2, 0.3 and 0.4) as potential agents for the miniaturization of high frequency antennas are presented. All the synthesized compositions were experimentally revealed to possess pure spinel phase. Dual-equivalent permeability and permittivity ($\mu' \approx 26$, $\varepsilon' \approx 25$, x = 0.3 and $\mu' \approx 29$, $\varepsilon' \approx 28$, x = 0.4) from 5 to 100 MHz can be achieved by introducing Cd^{2+} ions, yielding large miniaturization factors of up to 25 and 28. To figure out the effects of Cd^{2+} ions substitution on magnetic and dielectric properties, the change in microstructure is mainly investigated. Meanwhile, enhanced magnetic properties including upward saturation magnetization (*Ms*) (approximately 47.60 emu/g) and reduced coercivity (approximately 54.22 Oe) are obtained due to increased grain size and denser microstructure arrangements reflected from scanning electron microscopy images. With low magnitude order of magnetic and dielectric losses factors ($tan\delta_\varepsilon$ reaches 10^{-4}, $tan\delta_\mu$ reaches 10^{-2}), the composites can potentially exhibit high operating efficiencies at high frequencies.

1. Introduction

In order to achieve long distance and high speed of modern wireless communication, the necessity of developing antennas with compact size and high radiation efficiencies is essential [1–6]. Many approaches including reducing radiator size, by truncating corners and adopting high-refractive substrates with miniaturization factor N ($N = \sqrt{\mu\varepsilon}$, $N > 1$) (μ and ε represent permeability and permittivity, respectively) have been made to meet the above-mentioned requirements [7–11]. Regarding conventional dielectric substrate materials without magnetization, large n means large ε, which would in return degrade bandwidth and radiation performance of antennas for severe mutual coupling due to surface wave would be excited and trapped into substrate [12,13]. Thus, to introduce magnetic properties into utilized materials or to use materials with magnetic and dielectric properties is an effective method to balance the adverse impact for too large ε. Generally, the following equation demonstrates the correlation between bandwidth (BW) and μ and ε in antennas with magneto-dielectrics [14]:

$$BW \approx \frac{96\frac{h}{\lambda}\sqrt{\frac{\mu}{\varepsilon}}}{\sqrt{2}(4 + 17\sqrt{\mu\varepsilon})}$$

Where h is substrate thickness, and λ is the wave length. It indicates that if N is determined by μ and ε, BW is heavily dependent on the value of $\sqrt{\frac{\mu}{\varepsilon}}$. However, the operation frequency will decrease, if the value of μ is highly increased, according to Snoek's limit [15]:

$$f_r \propto \frac{1}{\mu}$$

Where f_r is resonant frequency. Therefore, it's best to choose substrate materials with moderate μ and ε.

Recently, low loss materials with magnetic and dielectric properties have attracted a lot of attention in the field of wireless communication for their excellent high-frequency characteristics [16–19]. Ferrites that have matching μ and ε in particular, have become popular due to their characteristic impedance (Z), which matches well with that of the transmitting medium, based on the following formula [20]:

* Corresponding author.
** Corresponding author.
E-mail addresses: dnzhang@uestc.edu.cn (D. Zhang), chenrt@austin.utexas.edu (R.T. Chen).

https://doi.org/10.1016/j.ceramint.2019.10.165
Received 7 September 2019; Received in revised form 12 October 2019; Accepted 17 October 2019
Available online 18 October 2019

$$Z = \sqrt{\frac{\mu'\mu_0'}{\varepsilon'\varepsilon_0'}} = \eta_0\sqrt{\frac{\mu'}{\varepsilon'}}$$

Where $\eta_0 = \sqrt{\frac{\mu_0'}{\varepsilon_0'}}$, represents the impedance of transmitting medium, and μ' and ε' represent real part of permeability and permittivity, respectively. Z and η_0 will be approximately equal if the value of μ' is closed to that of ε'. In such a case, electromagnetic signals can be transmitted well without reflection loss arising from a mismatch between radiator and medium, in the process of sending and receiving process of antennas. Some investigations have been carried out in this area. V.G. Harris with his group investigated Co–Ti substituted low loss M-type hexaferrite composites with tailored magneto-dielectric properties and therefore equivalent μ' and ε' were achieved [11]. In 2016, A. Saini et al. proposed ferrites with equivalent μ' and ε' by combining $Ni_{0.5}Zn_{0.3}Co_{0.2}Fe_2O_4$ with $BaFe_{12}O_{19}$, accompanied by a decrease in reflection loss (-35 dB to -28 dB) and an increase in bandwidth (1.6 %-6%) [10]. However, there were still not too many studies on such Mg ferrites, although they have great potential for many areas such as medical treatment, communication and sensing [21]. Meanwhile, as soft materials, their magnetic and dielectric properties are easy to tailor by other ions substituting Mg ions or Fe ions, through which equivalent μ' and ε' can also be realized. In our previous work, enhanced magnetic and dielectric properties of Bi_2O_3 doped Mg–Cd and In-doped Mg–Cd ferrites with low loss tangents and the influence of microstructure on magnetic and dielectric performance were symmetrically investigated for high frequency application [22–24].

The objective of the presented work is to study the effect of Cd ion substitution on the microstructure and crystalline phase of Mg composites, which further influences magnetic and dielectric performance, magnetization and low-loss properties. Consequently, the above effects for each Cd ion concentration are discussed and conclusions are drawn.

2. Experiment

The proposed spinel ferrites were synthesized using the conventional solid-state reaction method. The highly purified metallic oxide powders of analytical-grade MgO (AR grade, ≥ 99%), Fe_2O_3 (AR grade, ≥ 99%), Co_2O_3 (AR grade, ≥ 99%) and CdO (AR grade, ≥ 99%) were processed by weighing, mixing and first-time ball milling with deionized water using a planetary mixer for 10 h. Then, the milled slurries were dried and pre-sintered at 1000 °C for 4 h to form the primary phase. After undergoing ball milling for a second-time (for another 10 h) and then drying, the powders were pelletized with polyvinyl alcohol (PVA, 10 wt%) as a binder. The particles were pressed into fixed-size circular wafers and rings with a pressure of up to 10 MPa. Finally, the formed samples were sintered at 1100 °C for 4 h in the same sintering environment as that used in pre-sintering.

The crystallographic structures of the samples with various Cd ions concentrations were established by X-ray diffraction (XRD) studies (DX-2700, Haoyuan Co.), using Cu-Ka radiation, with a θ-2θ geometric angle rang of 20° to 120°. Rietveld refinement was then performed on the original XRD patterns to determine the crystalline structure and phase composition using GASA refinement software. In the duration of the refinement, the amount of Mg, Cd and Fe ions occupying at A-site were firstly assumed to be a, 1-a-b and b, respectively. Then the starting a value was assumed to be 0. Therefore, the distribution of ions at A-site and B-site can be calculated using the following cation distribution formula.

$$(Mg_aCd_{1-a-b}Fe_b)^A[Mg_{1-x-a}Cd_{x+y+b-1}Fe_{1.95-b}Co_{0.05}]^BO_4$$

Finally, the best fit Rietveld profiles, the difference between the observed pattern and the best-fit Rietveld profiles, cell parameters, theoretical density and Bragg peak positions were obtained by steps of fittings and iterations. The reliability parameters validated the reliability of Rietveld refinement.

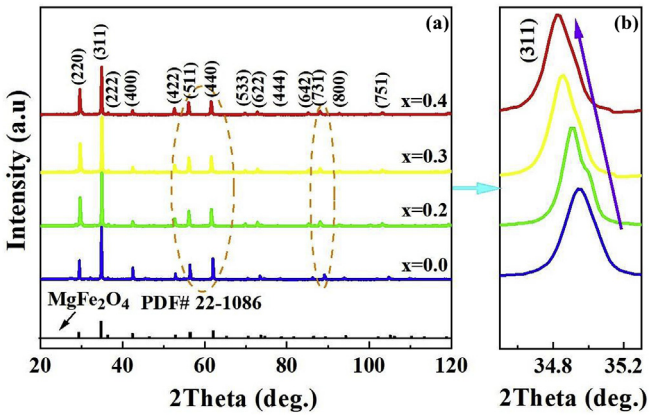

Fig. 1. XRD patterns of samples with various x values.

Complex magnetic permeability and permittivity of the samples were measured using a HP-42391B RF impedance analyzer, over a frequency band of 1 MHz to 1.5 GHz. Scanning electron microscopy (SEM), (JEOL, JSM-6490) was applied to magnify the photographic microstructure by a factor of 6000. The magnetic hysteresis loops were measured using a vibrating sample magnetometer (VSM), (MODEL, BHL-525) with an applied magnetic field scope of -5000 Oe to 5000 Oe. We conducted X-ray photoelectron spectroscopy (XPS) (Thermo Fisher Scientific K-Alpha, USA) with an Al–K excitation light source and a voltage of 5 kV to confirm the valence states of Fe ions. The fitting software XPSPESK 4.1 was then used to fit the measured results by deconvolution. Finally, the existence of valence states of bivalent and trivalent for Fe ions was detected. An auto density tester (GF-300D, AND Co.) was employed to measure the bulk density with Archimedes' principle. All the measurements were performed at normal room temperature around 30 °C.

3. Results and discussion

The crystal structures of synthesized ferrites with their XRD diffraction patterns are displayed in Fig. 1. It is observed that all the diffraction peaks when placed in proper positions reveal a norm spinel structure without an impurity phase, indexed to standard $MgFe_2O_4$ peaks as per JCPDS Card Files, no. 22–1086, Fd-3m (227). This means Cd ions have little influence on the crystalline structure of Mg ferrites. In samples when x increases from 0.0 to 0.4, there is a slight peak shift toward left observed for the samples with increasing Cd ions, especially peaks (511), (440) and (731) marked by orange ellipses, and enlarged peak (311) in Fig. 1 (b). This is because substituted Cd ions with larger ionic radius than that of Mg ions enlarge the cell parameters of the original Mg ferrites, as shown in Table 1.

Rietveld refinement was performed to determine the original XRD patterns and phase composition based on XRD diffraction data. And the results are shown in Fig. 2 and Table 1. Among them, Fig. 2 shows visualized schematic of the observed and the best-fit Rietveld profiles, which exports convinced patterns with well-matching, fitted and measured data. As exhibited in Table 1, the substituted Cd ions occupy tetrahedral (A) site despite the change in x, while the distribution of Mg/Fe cations at A site and octahedral (B) site depends on the amount of Cd ions substituted. This is because Mg ions occupy at both A site and B site without stationary distribution ratio, and the importation of Cd ions will result in change in their occupation. Our former investigation [25] also proved that the substitution for Cd cations influenced the occupation of Mg cations in the Mg ceramic ferrites. Meanwhile, with relatively low values of ωRp, Rp and χ^2 (listed in Table 1) extracted from the GASA software, the refinement confirms excellent reliability. Here, after comparing the refinement results with what we obtained in previous work [25], in which Bi_2O_3 additive was introduced, we find

Table 1
Rietveld refinement results for the X-ray diffraction patterns with ions at A site, B site, χ^2, ωRp, Rp, the occupation of Cd ions and cell parameter.

x value	A site	B site	χ^2	ωRp	Rp	Cd occupation	Cell parameter (Å)
0.0	(Mg2+ 0.7Fe3+ 0.3)	[Mg2+ 0.3Co3+ 0.05Fe3+ 1.65]O^{4-}	1.29	2.36%	1.73%	A site	8.4023
0.2	(Mg2+ 0.26Cd2+ 0.2Fe3+ 0.54)	[Mg2+ 0.54Co3+ 0.05Fe3+ 1.41]O4-	1.69	5.92%	3.43%	A site	8.4569
0.3	(Mg2+ 0.23Cd2+ 0.3Fe3+ 0.47)	[Mg2+ 0.47Co3+ 0.05Fe3+ 1.48]O^{4-}	1.44	3.87%	2.82%	A site	8.4863
0.4	(Mg2+ 0.2Cd2+ 0.4Fe3+ 0.4)	[Mg2+ 0.4Co3+ 0.05Fe3+ 1.55]O^{4-}	1.72	6.45%	4.53%	A site	8.5196

the occupation of cations at A site and B site is unmodifiable with and without additive.

The SEM micrographs of $Mg_{1-x}Cd_xCo_{0.05}Fe_{1.95}O_4$ (x = 0.0, 0.2, 0.3 and 0.4) ferrites with apparent spinel structure are shown in Fig. 3. It is observed that densification, grain size, and porosity depend heavily on the concentration of Cd ions. More prominent boundaries and denser microstructures can be observed as x increases. Especially when x rises up to 0.4, the sample reveals an excellent microstructure with far larger grain size and lower porosity. Regarding average grain size, it exhibits a monotone-increasing trend, with values of 1.12 μm, 1.93 μm, 3.20 μm and 9.31 μm corresponding to x values of 0.0, 0.2, 0.3, 0.4, respectively. It can be attributed to the larger ionic radius of Cd ions than that of Mg ions, as x increases, more concentration of Cd ions results in larger grain size. Meanwhile, higher densification with less holes emerging is also attained with higher x value. In order to explore the densification, the relative density (*RD*) is worked out and listed in Table 2. Here *RD* is calculated by the equation:

$$RD = \frac{ED}{TD}$$

Where *ED* is the experimental density measured by the auto density tester and *TD* is the theoretical density obtained in the Rietveld refinement. It is noticed that the relative densities are higher than 94.5% for all samples, and the *RD* increases with increasing Cd^{2+} concentration. It indicates that dense structure can be realized through the experimental method.

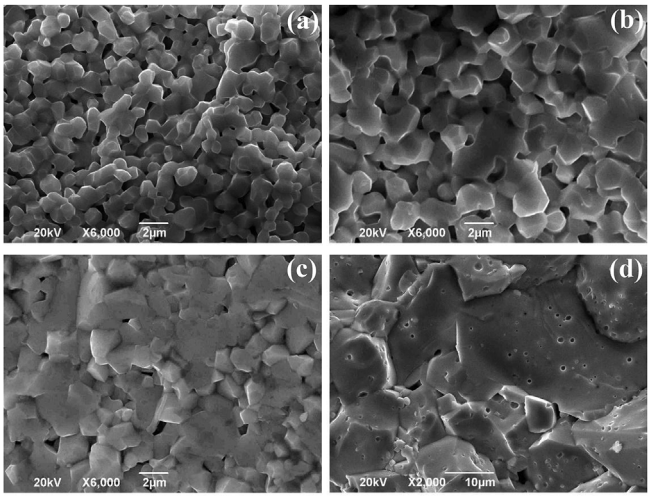

Fig. 3. Surface SEM micrographs of $Mg_{1-x}Cd_xCo_{0.05}Fe_{1.95}O_4$ ferrites. (a) x = 0.0; (b) x = 0.2; (c) x = 0.3 and (d) x = 0.4.

Fig. 4 shows magnetic hysteresis loops, saturation magnetization (*Ms*) and coercivity (*Hc*) of $Mg_{1-x}Cd_xCo_{0.05}Fe_{1.95}O_4$ composites with

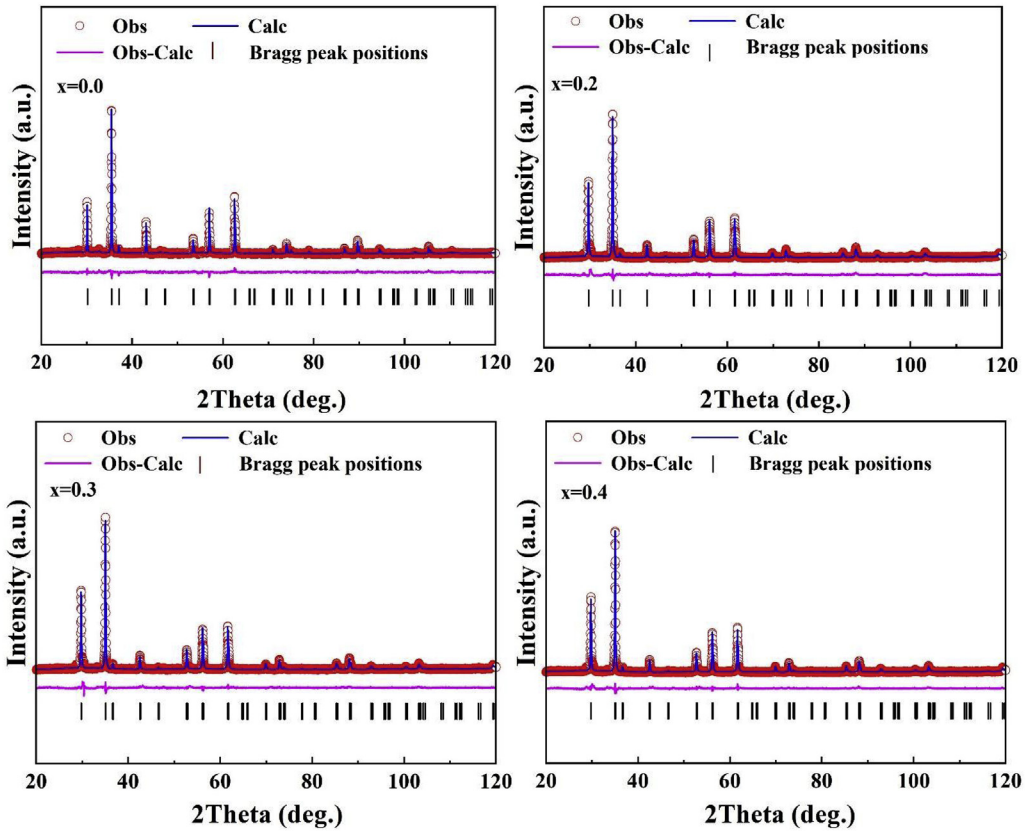

Fig. 2. Rietveld refinement results of the X-ray diffraction patterns of the samples with different x values. The observed patterns (red rings), the best fit Rietveld profiles (dashed lines in blue), and difference between the observed pattern and the best-fit Rietveld profiles (solid line in magenta), and Bragg peak positions of Mg ferrites (vertical segments in black). (For interpretation of the references to colour in this figure legend, the reader is referred to the Web version of this article.)

Table 2
Relative densities of samples with various sintering temperature points.

x value	0.0	0.2	0.3	0.4
relative densities	94.65%	94.87%	96.32%	96.98%

x = 0.0, 0.2, 0.3 and 0.4. it indicates the synthesized ferrites possess enhanced magnetization, which is applied for auxiliary interpretation of the change in permeability, as discussed below. Fig. 4 (a) illustrates that the synthesized samples possess excellent soft magnetic properties as a whole. The saturation magnetization (*Ms*) increases significantly from approximately 32.6 emu/g to 47.6 emu/g with increasing Cd ions concentration, as exhibited in Fig. 4 (b). Two factors are responsible for this change. On one hand, as x increases from 0.0 to 0.2, the enhancement in *Ms* is due to the substitution of non-magnetic Cd^{2+} ions for magnetic Mg^{2+} ions at A site, causes changeable super-exchange interaction via oxygen between A site and B site, where two corresponding crystallographic sublattices are exhibited [26]. The preferential occupation of Mg/Fe ions occupying at A site and B site lies on their affinity to some degree. In our experiment, as Table 1 illustrates, as x continuously increases from 0.2 to 0.4, there is a portion of Mg ions migrating from B-site to A-site while partial Fe ions migrate in reverse. As a result, surface exchange bonds are broken and A-B-site exchange interaction are weakened, causing reduced edge strain, canted spin orientation and increased *Ms* [27]. On the other hand, the preferable microstructures with larger grain size and denser arrangement also promote the magnetization [28]. It can be explained using the theory of a dead layer [29], in which it is assumed that magnetic particles are limited in a non-magnetic layer, as grains increase, the amount of dead layer decreases, resulting in increased *Ms*. Generally, through introducing a non-magnetic cation that can further tune their structural, electrical and magnetic, the ferrites can emerge more outstanding magnetic and dielectric properties [30]. As x increases, the coercivity (*Hc*) in Fig. 4 (b) changes in a direction opposite to that of *Ms*, with values drop from 71.87 Oe to 54.22 Oe. This is mainly due to the increase in grain size, as shown in SEM images. Decreased *Hc* means the required energy of domain-wall movement is less than that of domain rotation to achieve equal magnetization. Larger grain size means more domain walls, which can contribute more easily to the magnetization than domain rotation [31]. Thus, the larger grain size is, the lower *Hc* goes. Additionally, the negative correlation between *Ms* and *Hc* can be theoretically described by the Stoner-Wohlfarth theory [32].

$$Ms = \frac{0.96K_1}{Hc}$$

Where *K*1 is the anisotropy constant. This equation proves that the experimental changes in *Ms* and *Hc* are well consistent with the theoretical description.

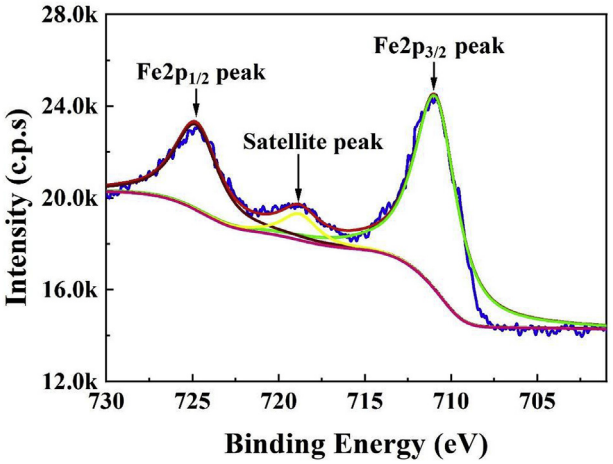

Fig. 5. Fe-2p XPS spectra of sample with x = 0.4.

To further investigate the reason of the changes in magnetization and dielectric properties pertaining to the valency of Fe ions (+2 and + 3) in the samples, XPS measurements are performed. All the samples display identical peaks and densities, so the sample with x = 0.4 is chosen to be characterized and graphed in Fig. 5, which shows the intensity of the Fe 2p peaks against binding energy. Consequently, it illustrates that all the Fe ions are in the +3 state and no +2 state are detected, as binding energy of 711.04 eV, 718.96 eV, and 724.9 eV in correspondence with the $Fe2p_{3/2}$ peak, satellite peak, and $Fe2p_{1/2}$ peak. Therefore, no contribution of Fe^{2+} to the *Hc* is ascertained. This was investigated because the concentration of Fe^{2+} plays a key role in determining loss factor and anisotropy constant, which are correlated to *Hc* as per the one-ion model [33].

Fig. 6 shows the change in complex permittivity and permeability as a function of applied frequency for the composition $Mg_{1-x}Cd_xCo_{0.05}Fe_{1.95}O_4$ with x = 0.0–0.4. Fig. 6 (a) shows the permittivity spectrum in the frequency range from 1 MHz to 1.5 GHz. The real part (ε') and imaginary part (ε'') of permittivity show a flat response with frequency covering 1 MHz to 800 MHz for all samples. The dielectric properties are enhanced when the concentrations of Cd ions are higher. This is reflected by a slight increase in the real part (ε') of permittivity, with values escalating approximately from 19 to 28 F/m, as x increases. This can be attributed to the microstructure with larger grain size and denser grain arrangement. Smaller surface boundaries are contained in larger grains that have more high-resistance areas. Thus, ε' increases due to the increase in the interfacial polarization [34]. Although the imaginary part (ε'') of permittivity shown exhibits the same variation tendency as ε' with the increasing value of x (as shown in Fig. 6 (a)), the values for ε'' are fairly low (~magnitude of $2*10^{-2}$) over a frequency

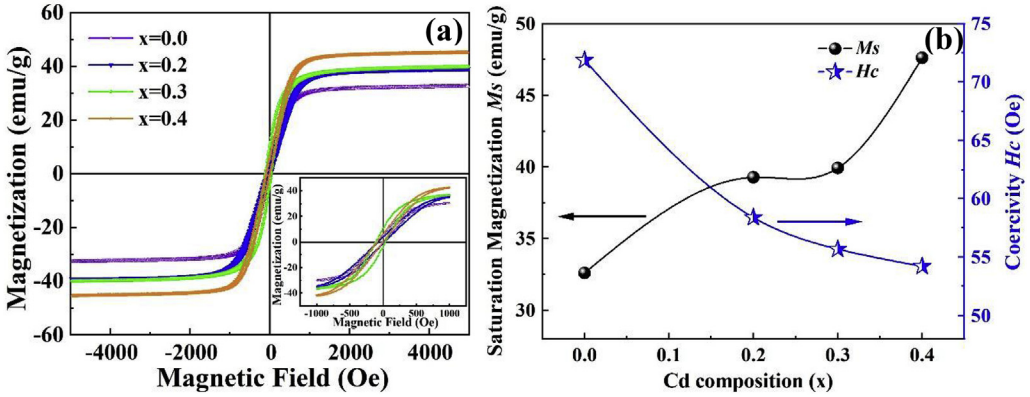

Fig. 4. Magnetic hysteresis loops (a) magnetic properties and (b) *Ms* and *Hc* of samples with various x values.

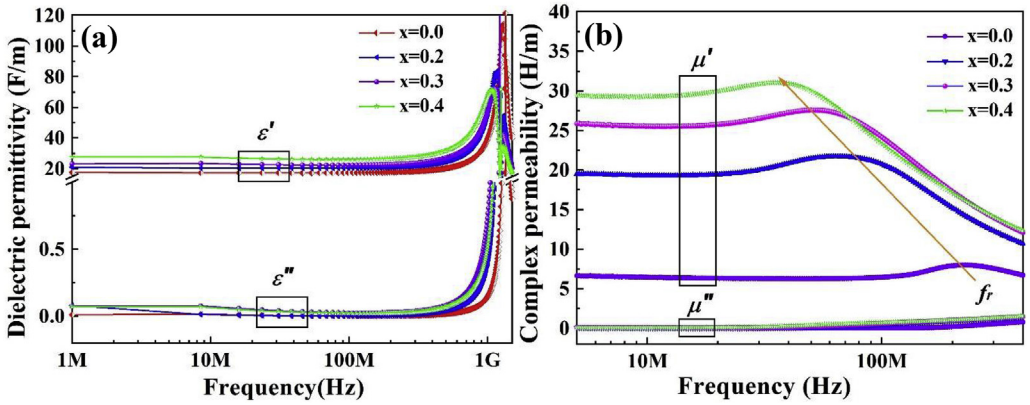

Fig. 6. (a) The complex dielectric permittivity (b) the complex magnetic permeability of the samples with various x values.

range of 5 to 500 MHz. Hereby, dielectric loss factor $tan\delta_\varepsilon$ can be determined according to the following equation [35].

$$tan\delta_\varepsilon = \frac{\varepsilon''}{\varepsilon'}$$

Consequently, magnitude order of $tan\delta_\varepsilon$ as low as $1*10^{-3}$ or even $7*10^{-4}$ for the $Mg_{1-x}Cd_xCo_{0.05}Fe_{1.95}O_4$ composites are obtained, and specific $tan\delta_\varepsilon$ for all samples at some frequency points are listed in Table 3. Here, microstructure is the main factor affecting $tan\delta_\varepsilon$, which can be attributed to the relationship below [36].

$$tan\delta_\varepsilon = (1-P)tan\delta_0 + CP^n$$

Where $tan\delta_0$ is complete-densification loss factor of corresponding materials, P ($0 < P < 1$) is the porosity and C is a constant. This equation indicates that $tan\delta_\varepsilon$ consists of two parts from intrinsic and external view, of which $(1\text{-}P)tan\delta_0$ represents intrinsic loss relying on P, which results from the synthesis of the material and CP^n represents external loss, which can always be ignored for a relatively large value of n.

The variation of the complex permeability, depending on the concentration of Cd^{2+} ions, is given in Fig. 6 (b). It can be seen the real part of permeability (μ') monotonically increase by a large margin from approximately 7 to 29 H/m. This is because μ' is directly proportional to Ms and grain size, the relationships are summarized by the following equation [37].

$$\mu \propto \frac{Ms^2 D_m}{K}$$

Where K denotes the magneto-crystalline anisotropy constant, and D_m is the average size. As discussed with increased Ms and D_m, μ will increase obviously. Additionally, an apparent shift of resonant frequency (f_r) of μ' towards lower frequency direction with higher concentration of Cd^{2+} substitution is observed due to the Snoek's limit [38]. This explains why μ should not be design that large from another point of view.

The imaginary part (μ'') of permeability for all samples shown in Fig. 6 (b) remains as low as approximately 0.5 over the experimental frequency range. Therefore, the magnetic loss factor ($tan\delta_\mu$) can be calculated to be $2*10^{-2}$ by $\frac{\mu''}{\mu'}$, and numerical $tan\delta_\mu$ values are still exposed in Table 3. Three factors result in low magnetic loss factor, the eddy current loss $tan\delta_e$, the hysteresis loss $tan\delta_a$ and the residual loss $tan\delta_c$, as summarized by the following relationship [39].

$$tan\delta_\mu = tan\delta_e + tan\delta_a + tan\delta_c$$

Thus, $tan\delta_e$ depends on the electrical resistivity. The value of $tan\delta_a$ closely correlates to Hc, due to electro-magnetic induction, which is the key to generate fever and power dissipation. The value of $tan\delta_e$ can be lowered by optimizing the microstructure by promoting grain growing or increasing the grain arrangement density. The last factor, $tan\delta_c$ is small and related to domain wall and spin rotational resonances. In our study, low magnetic loss is obtained due to lowered Hc and hysteresis loop area resulting from the densification-sintered microstructure by doping Cd^{2+} ions.

The property of equivalent μ' and ε' with normalized characteristics impedance ($Z \approx 1$) and miniaturization factor (N) extracted and calculated from Fig. 6 for the synthesized composites with x = 0.3 and 0.4 are shown in Fig. 7. It is observed that that Z is closed to 1 for both sintered ferrites over the frequency range from 5 MHz to 100 MHz. This is due to nearly equal μ' and ε'. Thus, matching impedance between the substrate materials and propagation medium can be achieved. In addition, the values of N are around 25 and 28 for the samples where x = 0.3 and 0.4, meaning high miniaturization factors are attained as well.

Table 3
$tan\delta_\varepsilon/tan\delta_\mu$ values at frequency points of 10 MHz, 50 MHz and 100 MHz for $Mg_{1-x}Cd_xCo_{0.05}Fe_{1.95}O_4$ composites with various x values.

x value	$tan\delta_\varepsilon/tan\delta_\mu$ @ 10 MHz	$tan\delta_\varepsilon/tan\delta_\mu$ @ 50 MHz	$tan\delta_\varepsilon/tan\delta_\mu$ @ 100 MHz
0.0	$1.7*10^{-3}/8.5*10^{-2}$	$4.9*10^{-3}/4.3*10^{-2}$	$2.8*10^{-3}/3.7*10^{-2}$
0.2	$1.4*10^{-3}/4.4*10^{-3}$	$3.8*10^{-3}/3.7*10^{-2}$	$3.4*10^{-3}/4.8*10^{-2}$
0.3	$7.8*10^{-4}/5.9*10^{-2}$	$1.3*10^{-3}/3.1*10^{-2}$	$1.0*10^{-3}/6.1*10^{-2}$
0.4	$7.1*10^{-4}/5.6*10^{-2}$	$3.0*10^{-3}/3.8*10^{-2}$	$2.2*10^{-3}/7.2*10^{-2}$

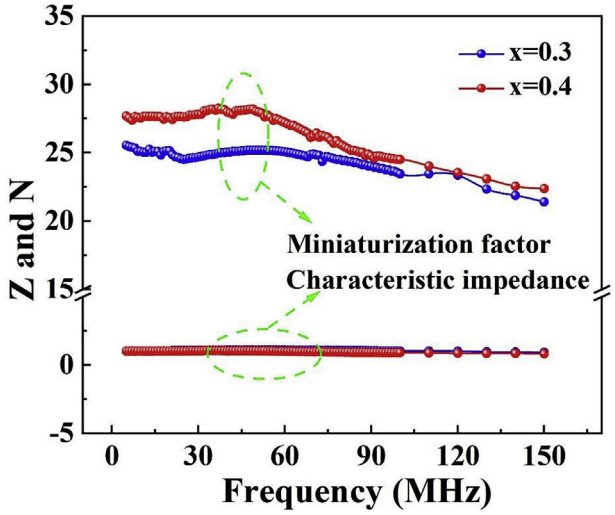

Fig. 7. Miniaturization factors and characteristics impedances of $Mg_{1-x}Cd_xCo_{0.05}Fe_{1.95}O_4$ composites with x = 0.3 and x = 0.4.

4. Conclusion

We propose increased permeability and permittivity, low loss and high miniaturization of Mg spinel ferrites by substituting Mg ions with Cd ions at tetrahedral site. Experimentally, the results demonstrate that the substitution of Cd^{2+} for Mg^{2+} favorably promotes an enhancement in magnetization and imposes a restriction on coercivity. Meanwhile, higher concentration of Cd^{2+} ions helps to tailor the permeability and permittivity to be nearly equal for two values of x. Consequently, dual-equivalent permeability and permittivity ($\mu' \approx 26$, $\varepsilon' \approx 25$, $x = 0.3$ and $\mu' \approx 29$, $\varepsilon' \approx 28$, $x = 0.4$) with corresponding high miniaturization factors (25 and 28) are obtained. Additionally, preferable microstructure facilitated by addition of Cd^{2+} gives rise to extremely low loss factors ($tan\delta_{\varepsilon}$ reaches 10^{-4}, $tan\delta_{\mu}$ reaches 10^{-2}). The reported results exhibit remarkable improvements over some previous researches.

Declaration of competing interest

The authors declare that they have no known competing financial interests or personal relationships that could have appeared to influence the work reported in this paper.

Acknowledgements

This work was supported by National Key Scientific Instrument and Equipment Development Project No.51827802, and by the National Natural Science Foundation of China (Nos. 51602036 and 51872041).

References

[1] Z. Gan, Z.H. Tu, Z.M. Xie, Q.X. Chu, Y. Yao, Compact wideband circularly polarized microstrip antenna array for 45 GHz application, IEEE Trans. Antennas Propag. (2018), https://doi.org/10.1109/TAP.2018.2863243.
[2] S. Xiumei, Y. Liu, L. Zhao, G.-L. Huang, X. Shi, Q. Huang, A miniaturized microstrip antenna array at 5G millimeter wave band, IEEE Antennas Wirel. Propag. Lett. 18 (2019), https://doi.org/10.1109/LAWP.2019.2927460 1–1.
[3] Z. Shao, Y.P. Zhang, Miniaturization of differentially-driven microstrip planar inverted F antenna, IEEE Trans. Antennas Propag. 67 (2019) 1280–1283, https://doi.org/10.1109/TAP.2018.2883575.
[4] K.K. So, H. Wong, K.M. Luk, C.H. Chan, Miniaturized circularly polarized patch antenna with low back radiation for GPS satellite communications, IEEE Trans. Antennas Propag. 63 (2015) 5934–5938, https://doi.org/10.1109/TAP.2015.2488000.
[5] L. Liu, C. Liu, Z. Li, X. Yin, Z.N. Chen, Slit-slot line and its application to low cross-polarization slot antenna and mutual-coupling suppressed tripolarized MIMO antenna, IEEE Trans. Antennas Propag. 67 (2019) 4–15, https://doi.org/10.1109/TAP.2018.2876166.
[6] P.J. Gogoi, M.M. Rabha, S. Bhattacharyya, N.S. Bhattacharyya, Miniaturization of body worn antenna using nano magneto-dielectric composite as substrate in C-band, J. Magn. Magn. Mater. 414 (2016) 209–218, https://doi.org/10.1016/j.jmmm.2016.04.016.
[7] M. Li, K.M. Luk, L. Ge, K. Zhang, Miniaturization of magnetoelectric dipole antenna by using metamaterial loading, IEEE Trans. Antennas Propag. 64 (2016) 4914–4918, https://doi.org/10.1109/TAP.2016.2599176.
[8] D. Wang, H. Wong, C.H. Chan, Small patch antennas incorporated with a substrate integrated irregular ground, IEEE Trans. Antennas Propag. 60 (2012) 3096–3103, https://doi.org/10.1109/TAP.2012.2196915.
[9] H. Wong, K.K. So, K.B. Ng, K.M. Luk, C.H. Chan, Q. Xue, Virtually shorted patch antenna for circular polarization, IEEE Antennas Wirel. Propag. Lett. 9 (2010) 1213–1216, https://doi.org/10.1109/LAWP.2010.2100361.
[10] A. Saini, K. Rana, A. Thakur, P. Thakur, J.L. Mattei, P. Queffelec, Low loss composite nano ferrite with matching permittivity and permeability in UHF band, Mater. Res. Bull. 76 (2016) 94–99, https://doi.org/10.1016/j.materresbull.2015.12.002.
[11] Y. Peng, X. Wu, Z. Chen, W. Liu, F. Wang, X. Wang, Z. Feng, Y. Chen, V.G. Harris, BiFeO 3 tailored low loss M-type hexaferrite composites having equivalent permeability and permittivity for very high frequency applications, J. Alloy. Comp. 630 (2015) 48–53, https://doi.org/10.1016/j.jallcom.2015.01.026.
[12] S. Sahandabadi, S.V.A.D. Makki, Mutual coupling reduction using complementary of SRR with wire MNG structure, Microw. Opt. Technol. Lett. 61 (2019) 1231–1234, https://doi.org/10.1002/mop.31717.
[13] N.H.M. Yunus, J. Yunas, A. Pawi, Z.A. Rhazali, J. Sampe, Investigation of micromachined antenna substrates operating at 5 GHz for RF energy harvesting applications, Micromachines 10 (2019), https://doi.org/10.3390/mi10020146.
[14] R.C. Hansen, M. Burke, Antennas with magneto-dielectrics, Microw. Opt. Technol. Lett. 26 (2000) 75–78, https://doi.org/10.1002/1098-2760(20000720)26:2<75::AID-MOP3>3.0.CO;2-W.
[15] J. Lee, J. Heo, J. Lee, Y. Han, Design of small antennas for mobile handsets using magneto-dielectric material, IEEE Trans. Antennas Propag. 60 (2012) 2080–2084, https://doi.org/10.1109/TAP.2012.2186271.
[16] A. Saini, P. Kumar, B. Ravelo, S. Lallechere, A. Thakur, P. Thakur, Magneto-dielectric properties of doped ferrite based nanosized ceramics over very high frequency range, Eng. Sci. Technol. an Int. J. 19 (2016) 911–916, https://doi.org/10.1016/j.jestch.2015.12.008.
[17] Y. Yang, J. Li, H. Zhang, G. Wang, Y. Rao, G. Gan, TiO2 tailored low loss NiCuZn ferrite ceramics having equivalent permeability and permittivity for miniaturized antenna, J. Magn. Magn. Mater. 487 (2019) 165318, https://doi.org/10.1016/j.jmmm.2019.165318.
[18] M. Aldrigo, A. Costanzo, D. Masotti, C. Galassi, Exploitation of a novel magneto-dielectric substrate for miniaturization of wearable UHF antennas, Mater. Lett. 87 (2012) 127–130, https://doi.org/10.1016/j.matlet.2012.07.101.
[19] K. Borah, N.S. Bhattacharyya, Magnetodielectric composite with ferrite inclusions as substrates for microstrip patch antennas at microwave frequencies, Compos. B Eng. 43 (2012) 1309–1314, https://doi.org/10.1016/j.compositesb.2011.11.067.
[20] Y. Lin, X. Liu, H. Yang, F. Wang, C. Liu, X. Wang, Laminated SrTiO3-Ni0.8Zn0.2Fe2O4magneto-dielectric composites for high frequency applications, J. Alloy. Comp. (2016), https://doi.org/10.1016/j.jallcom.2016.07.225.
[21] T. Krishnaveni, S.R. Murthy, F. Gao, Q. Lu, S. Komarneni, Microwave hydrothermal synthesis of nanosize Ta2O5 added Mg-Cu-Zn ferrites, J. Mater. Sci. 41 (2006) 1471–1474, https://doi.org/10.1007/s10853-006-7488-5.
[22] G. Gan, H. Zhang, Q. Li, J. Li, X. Huang, F. Xie, F. Xu, Q. Zhang, M. Li, T. Liang, G. Wang, Low loss, enhanced magneto-dielectric properties of Bi 2 O 3 doped Mg-Cd ferrites for high frequency antennas, J. Alloy. Comp. (2018), https://doi.org/10.1016/j.jallcom.2017.12.002.
[23] G. Gan, D. Zhang, Q. Zhang, G. Wang, X. Huang, Y. Yang, Y. Rao, J. Li, F. Xu, X. Wang, R.T. Chen, H. Zhang, Influence of microstructure on magnetic and dielectric performance of Bi 2 O 3 -doped Mg[sbnd]Cd ferrites for high frequency antennas, Ceram. Int. (2019), https://doi.org/10.1016/j.ceramint.2019.03.098.
[24] J. Li, D. Wen, Q. Li, T. Qiu, G. Gan, H. Zhang, Equal permeability and permittivity in a low temperature co-fired In-doped Mg-Cd ferrite, Ceram. Int. 44 (2018), https://doi.org/10.1016/j.ceramint.2017.09.228.
[25] G. Gan, H. Zhang, Q. Li, J. Li, X. Huang, F. Xie, F. Xu, Q. Zhang, M. Li, T. Liang, G. Wang, Low loss, enhanced magneto-dielectric properties of Bi_2O_3doped Mg-Cd ferrites for high frequency antennas, J. Alloy. Comp. 735 (2018), https://doi.org/10.1016/j.jallcom.2017.12.002.
[26] M.H. Mahmoud, A.M. Elshahawy, S.A. Makhlouf, H.H. Hamdeh, Synthesis of highly ordered 30 nm NiFe2O4 particles by the microwave-combustion method, J. Magn. Magn. Mater. 369 (2014) 55–61, https://doi.org/10.1016/j.jmmm.2014.06.011.
[27] M. Younas, M. Nadeem, M. Atif, R. Grossinger, Metal-semiconductor transition in NiFe 2 O 4 nanoparticles due to reverse cationic distribution by impedance spectroscopy, J. Appl. Phys. 109 (2011), https://doi.org/10.1063/1.3582142.
[28] A. Manikandan, J. Judith Vijaya, L. John Kennedy, M. Bououdina, Microwave combustion synthesis, structural, optical and magnetic properties of Zn1-xSrxFe2O4 nanoparticles, Ceram. Int. (2013), https://doi.org/10.1016/j.ceramint.2013.01.012.
[29] R.S. Yadav, I. Kuřitka, J. Vilcakova, J. Havlica, J. Masilko, L. Kalina, J. Tkacz, V. Enev, M. Hajdúchová, Structural, magnetic, dielectric, and electrical properties of NiFe2O4 spinel ferrite nanoparticles prepared by honey-mediated sol-gel combustion, J. Phys. Chem. Solids (2017), https://doi.org/10.1016/j.jpcs.2017.04.004.
[30] S.S. Thakur, A. Pathania, P. Thakur, A. Thakur, J.H. Hsu, Improved structural, electrical and magnetic properties of Mn-Zn-Cd nanoferrites, Ceram. Int. 41 (2015) 5072–5078, https://doi.org/10.1016/j.ceramint.2014.12.077.
[31] M.T. Farid, I. Ahmad, M. Kanwal, G. Murtaza, I. Ali, S.A. Khan, The role of praseodymium substituted ions on electrical and magnetic properties of Mg spinel ferrites, J. Magn. Magn. Mater. 428 (2017) 136–143, https://doi.org/10.1016/j.jmmm.2016.12.031.
[32] S.E. Shirsath, S.S. Jadhav, B.G. Toksha, S.M. Patange, K.M. Jadhav, Influence of Ce4 ions on the structural and magnetic properties of NiFe2O4, J. Appl. Phys. 110 (2011), https://doi.org/10.1063/1.3603004.
[33] A.B. Gadkari, T.J. Shinde, P.N. Vasambekar, Magnetic properties of rare earth ion (Sm 3+) added nanocrystalline Mg-Cd ferrites, prepared by oxalate co-precipitation method, J. Magn. Magn. Mater. 322 (2010) 3823–3827, https://doi.org/10.1016/j.jmmm.2010.06.021.
[34] G. Sathishkumar, C. Venkataraju, K. Sivakumar, Magnetic and dielectric properties of cadmium substituted nickel cobalt nanoferrites, J. Mater. Sci. Mater. Electron. 24 (2013) 1057–1062, https://doi.org/10.1007/s10854-012-0878-3.
[35] M.A. Dar, D. Varshney, Effect of d-block element Co2+ substitution on structural, Mössbauer and dielectric properties of spinel copper ferrites, J. Magn. Magn. Mater. 436 (2017) 101–112, https://doi.org/10.1016/j.jmmm.2017.04.046.
[36] H. Jia, W. Liu, Z. Zhang, F. Chen, Y. Li, J. Liu, Y. Nie, Monodomain MgCuZn ferrite with equivalent permeability and permittivity for broad frequency band applications, Ceram. Int. 43 (2017) 5974–5978, https://doi.org/10.1016/j.ceramint.2017.01.129.
[37] B.S. Chauhan, R. Kumar, K.M. Jadhav, M. Singh, Magnetic study of substituted mg-mn ferrites synthesized by citrate precursor method, J. Magn. Magn. Mater. 283 (2004) 71–81, https://doi.org/10.1016/j.jmmm.2004.04.133.
[38] Y. Bai, J. Zhou, Z. Gui, L. Li, L. Qiao, The physic properties of Bi-Zn codoped Y-type hexagonal ferrite, J. Alloy. Comp. 450 (2008) 412–416, https://doi.org/10.1016/j.jallcom.2006.10.122.
[39] Y. Peng, X. Wu, Z. Chen, Q. Li, T. Yu, Z. Feng, Z. Su, Y. Chen, V.G. Harris, High frequency permeability and permittivity spectra of BiFeO3/(CoTi)-BaM ferrite composites, J. Appl. Phys. 117 (2015) 1–5, https://doi.org/10.1063/1.4907331.